Ion-induced nucleation: Measurement of the effect of embryo's size and charge state on the critical supersaturation

Manuel Gamero-Castaño
Busek Co. Inc., Natick, Massachusetts 01760

Juan Fernández de la Mora
Department of Mechanical Engineering, Yale University, New Haven, Connecticut 06520

(Received 17 January 2002; accepted 17 May 2002)

We use 42 different charged nanoparticles generated by electrospray ionization and a differential mobility analyzer of unusual resolving power, as well as a condensation chamber of the turbulent-mixing type to study the dependence between the diameter, charge state, and critical supersaturation of embryos promoting heterogeneous nucleation. The nanoparticles investigated have diameters ranging from 0.43 to 6.51 nm, and positive charge states varying between 1 and 5 elementary units. We find that the critical supersaturation of small singly charged ions (mobility diameters bellow 1.01 nm) is independent of their size and its value coincides with the result anticipated by Thompson in his theory of ion-induced nucleation. On the other hand, the supersaturation required to activate multiply charged embryos is consistently higher than Thomson's prediction. In fact, the reduction of the critical supersaturation induced by electrification is much smaller than expected for large and multiply charged embryos, and their critical radius is estimated better by Kelvin's criterion. We speculate that this discrepancy is due to the geometrical differences between the actual nucleation sites and the idealized embryo considered in Thomson's model. [DOI: 10.1063/1.1492279]

I. INTRODUCTION

Heterogeneous nucleation is a class of nucleation phenomena in which foreign embryos favor the nucleation of vapors by acting as condensation sites. Ion-induced nucleation is a particular type of heterogeneous nucleation: bare ions, or more generally electrically charged nanoparticles, are the condensation embryos, and the strong ion-dipole interaction between them and the vapor molecules reduces the supersaturation required to promote nucleation. Heterogeneous and ion-induced nucleation play a major role in natural processes such as the generation of cloud droplets,[1] aerosol pollutants (e.g., acid rain), or the formation of tropospheric aerosol prompted by cosmic radiation.[2] Heterogeneous nucleation is also the working mechanism behind the condensation nucleus counter, an analytical instrument used to count individual aerosol nanoparticles by detecting optically the microscopic droplets condensed around them.[3] Thus, a good understanding of heterogeneous nucleation is important in areas of the atmospheric sciences and nanoparticle technology. At a more fundamental level, these phenomena have also been used to advance our knowledge of molecular interactions. In particular, the central electrostatic force typical of ion-induced nucleation makes it possible to devise simple analytical models for interactions at the molecular scale, and which can be experimentally verified.

The condensation of a supersaturated vapor around charged nanoparticles is largely an all-nothing process: the activation of the overwhelming fraction of a population of identical embryos occurs within a narrow window of the vapor's supersaturation, and a critical value S^* can be associated with the nucleation. A negligible fraction of the embryos are activated bellow S^*, while most of them grow into visible droplets when the saturation is increased above S^*. The critical supersaturation depends on the physical properties of the vapor, the temperature of the system, and the interaction forces between vapor molecules and embryo. A simplified model for the interactions consists of considering the ion-dipole potential only, along with the assumption that the embryo has spherical symmetry. This is the basis of Thomson's theory for ion-induced nucleation.[4] Despite some shortcomings (e.g., Thomson's theory cannot explain the observed dependence of the charge sign on the nucleation of some vapors[5]), this model has the advantage of reducing the number of variables entering in the problem (the size and charge state are the only properties of the embryo that influence S^*), and hence it has been considered a good, approximate criterion to estimate the critical supersaturation of charged nanoparticles. Finally, it must be pointed out that although the study of ion-induced nucleation on basis of S^* is relevant for practical applications, it does not yield a complete picture of the nucleation phenomena. In particular, it does not reveal that the nucleation of small ions is an activated process controlled by an energy barrier or explains the role played by stable solvated clusters in the transition from a small bare embryo into a droplet of critical size.[6,7]

Most of the research on ion-induced nucleation has been done with cloud chambers.[8,9] Although this technique is characterized by well-defined vapor concentration and temperature fields, it has been traditionally handicapped by the limited control of the properties of the nucleation embryos. These nucleation embryos are usually generated within the cloud chamber, by ionizing the background gas with ener-

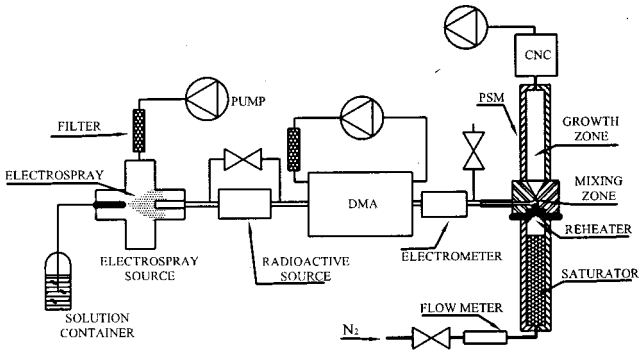

FIG. 1. Sketch of the experimental setup.

getic particles emitted from a radioactive source. This process makes it difficult to characterize and control the embryos, which is necessary to gain a better understanding of the nucleation phenomena. This shortcoming has been recently solved with the coupling of resonant-enhanced multiphoton ionization (REMPI) with the cloud chamber technique, and the study of well-defined ions is now possible.[10,11]

This paper presents measurements of the critical supersaturation of dibutyl phthalate vapors condensing around positively charged nanoparticles with mobility diameters ranging from 0.43 to 6.51 nm, and having up to 5 unit charges. A characterization of ion-induced nucleation in this broad window of embryos' sizes and charge states has not been reported previously. Furthermore, we will utilize the data of S^*, size, and charge of the embryos to test the validity of Thomson's equation. We will use the experimental approach first implemented by Seto *et al.*:[12] the charged nanoparticles serving as nucleation sites are generated with the electrospray ionization technique, and a differential mobility analyzer of unique resolution is employed to determine accurately their diameters and charge states. After the characterization of these two properties, the nanoparticle is introduced inside a nucleation chamber and its critical supersaturation measured. The nucleation chamber is an improved version of the turbulent-mixing type CNC used by Seto *et al.*[12,13] The article is organized as follows: after this introductory section we describe the experimental arrangement, the diagnostic techniques, and the nature of the nucleation embryos. The discussion of the main experimental findings is given in Sec. III. We will present the experimental data, comment succinctly on Thomson's theory, and analyze the data with the help of this model. The article then ends with some brief conclusions.

II. EXPERIMENT

A schematic of the experimental setup is shown in Fig. 1. The main elements are an electrospray source, a radioactive source, a differential mobility analyzer (DMA), and a nucleation chamber (PSM). The electrospray source is a handy tool to generate aerosols of charged droplets with a narrow-size distribution. A detailed description of similar sources and the principles behind the so-called cone-jet electrospraying mode can be found in the specialized literature.[14–16] After a sequence of steps that include evaporation of the liquid phase, Coulomb explosions, and ion field evaporation, the original droplets yield a variety of particles of different sizes and charge states (singly charged ions, singly and multiply charged cluster ions, dry residues, etc.).[17] The nanoparticles of this aerosol will become the nucleation embryos in which the present research is based. The residence time of the flow between the electrospray and radioactive sources is large enough to decompose the liquid droplets into a fully evolved, stable aerosol.

The radioactive source (Nuclespot Local Air Ionizer, model P-2042, 5 mCi, NRD, Grand Island, NY) generates alpha particles with enough kinetic energy to ionize partially the background gas, which in turn reduces the net charge of the incoming nanoparticles. We have the freedom to neutralize the aerosol at different degrees or maintain its original charging by forcing its flow to bypass the polonium source. Partial neutralization of the aerosol is convenient for two reasons: first, the nanoparticles of interest in this study and larger dry residues coexist in the same mobility range, which makes it difficult to analyze the embryos. Upon partial neutralization of the aerosol the position of the dry residues shifts towards smaller values of the mobility, while most nanoparticles keep their charge (the dry residues, holding a much larger amount of charge, are neutralized preferentially). This clarifies the mobility window occupied by the sought nanoparticles. Second, measuring the critical supersaturation associated with nanoparticles of the same size and different charge states is important in this investigation. This can be accomplished by partially discharging a nanoparticle that originally holds a few unit charges.

A key requirement for this study is the precise knowledge of the charge state and diameter of the nucleation embryos. This information is obtained with a differential mobility analyzer of the Eichler type.[18] The output signal of the DMA together with the working parameters (electric field and dimensions of the DMA channel, and flow rate of sheath gas) yields the electrical mobility spectrum of the aerosol, and a modified version of Millikan's formula for a sphere in free molecular regime can be used to establish a relation between the electrical mobility (Z), diameter (D), and charge (q) of a particle:[19]

$$Z = 0.44 \frac{q(k_B T/m)^{1/2}}{p(d_0 + D)^2}. \tag{1}$$

In this formula k_B is the Boltzmann constant, and m, p, and T stand for the molecular mass, the pressure, and the temperature of the sheath gas. This expression takes into account the finite diameter (d_0) of the gas molecules, and we will use the value given by de la Mora *et al.*, $d_0 = 0.53$ nm, to estimate this parameter.[20] Note that the knowledge of Z does not determine q and D independently. However, for particles with just a few unit charges, several procedures can be used to deduce their charge state unequivocally, and their diameters then follow from expression (1). These procedures include partial neutralization and the dependence between S^* and q for particles of the same size and different charge states.[13]

We use two different detectors, an electrometer of high sensitivity, and a particle-size-magnifier/condensation-nucleus-counter (PSM/CNC), to measure at the exit of the

TABLE I. Physical properties of DBP (T in °C).

Molecular weight (g/mol)	278.35
Density (g/cm^3)	$1.063-0.000826T$
Surface tension (dyn/cm)	$35.3-0.0863T$
Equilibrium vapor pressure p (mm Hg)	$1\mathrm{n}p=16.27-5099.0/(T+163.64)$
Dielectric constant	6.436 (30°C)

DMA the fraction of the aerosol with a given electrical mobility. The reading of the electrometer offers a deficient picture of the aerosol because the signal associated with a particle is proportional to its charge. Thus, for mobility values in which ions, cluster ions, and other small nanoparticles coexist with larger and highly charged dry residues, the electrometer signal barely reveals the presence of the former, as they appear buried under the background associated with the larger residues. Still, the electrometer serves to obtain a first picture of the aerosol and to determine the mobility of small and very mobile ions, which show as isolated peaks. On the other hand, the combination of PSM and CNC does count individual particles and therefore yields a better image of the components of the aerosol. The PSM is, essentially, a nucleation chamber with a controllable saturation level of the condensing vapor. Thus, the nanoparticles injected in the PSM become nucleation centers and grow into liquid droplets at the appropriate supersaturation, which is a function of the size and charge of the nanoparticle. Measuring such dependence is the objective of this work. Once the nanoparticle becomes a larger droplet, it can be counted with a commercial CNC (TSI model 3760, St Paul, MN; nominal detection size limit ~10 nm). The CNC simply functions as an optical counter: it only detects those nanoparticles that have been activated by the PSM. In fact, even the largest particles of the sprays characterized in this article are smaller than the detection limit of the commercial CNC.

The PSM is an evolution of the original design of Okuyama *et al.*,[21] and a detailed description can be found in the work of Gamero-Castaño and de la Mora.[13] A cold stream of ambient air carrying the aerosol and a hot stream formed by nitrogen and vapors of dibutyl phthalate (DBP) mix turbulently inside a long and narrow chamber (mixing zone). The relevant physical properties of DBP are given in Table I.[12] The temperature of the walls of the mixing chamber, as well as the temperature of the incoming aerosol, is regulated with a cooling jacket using water, commonly at 10 °C, as refrigerant fluid. The mixing of the cold and hot flows creates an environment with high values of the DBP saturation. Previously to its entrance into the mixer, the flow of nitrogen is passed through a bed of silica gel soaked with DBP (saturator). The temperature of the saturator is varied and controlled with a set of heat bands and temperature controllers. The time of residence of the nitrogen in this section of the PSM is large enough to saturate the nitrogen with DBP vapors at the temperature of the saturator. Thus, the molar flow rate of DBP ($\dot{n}_{DBP}$) exiting the saturator is given by

$$\dot{n}_{DBP}=\frac{Q_N P_{DBP}(T_S)}{R_g T_I}\frac{P_I}{P_I-P_{DBP}(T_S)}\cong\frac{Q_N P_{DBP}(T_S)}{R_g T_I}, \quad (2)$$

where P_I, T_I, and Q_N are the pressure, temperature, and volumetric flow rate of the nitrogen stream entering the saturator, $P_{DBP}(T_S)$ is the vapor pressure of DBP at the temperature of the saturator, and R_g is the universal gas constant. To avoid condensation of the vapors between the top of the saturator and the point of injection in the mixing chamber, the mixture of nitrogen and DBP is passed through an intermediate piece (reheater) at a temperature higher than T_S. Although the DBP vapors become undersaturated, the net amount of dibutyl phthalate injected in the mixer, which is the quantity needed to compute the critical supersaturation, is still given by Eq. (2). In fact, the saturation in the mixing chamber, or ratio between the partial pressure of DBP and its equilibrium vapor pressure at the mixing chamber conditions, is equal to

$$S^*=\frac{\dot{n}_{DP}R_g T_O}{Q_O P_{DBP}(T^*)}\cong\frac{Q_N}{Q_O}\frac{P_{DBP}(T_S)}{P_{DBP}(T^*)}. \quad (3)$$

In this expression T_O and Q_O are the temperature and flow rate of the gas entering the CNC (Q_O is 2.36×10^{-5} m^3 s^{-1}). T^* is the temperature at which the nucleation occurs. Q_N is measured with a flow meter located at the entrance of the saturator, and typical values are in the range 0 to 4×10^{-6} m^3 s^{-1}. A bleeding valve at the aerosol input keeps the PSM at atmospheric pressure. The nucleation temperature T^* is measured directly with a thermocouple inserted inside the mixing channel. The measurement of the thermocouple, which yields an averaged temperature of the mixing channel cross section, varies modestly along the axial coordinate of the channel, exhibiting a minimum at approximately 4 mm downstream the injection points. We will use this minimum as a fair estimate for T^*. Finally, note that the expression (3) is associated with equilibrium conditions and does not imply that the supersaturation in the mixing chamber is a uniform and steady scalar field. However, this is a good approximation because the turbulent mixing does create a high degree of homogeneity along the mixing chamber, except in narrow boundary layers on the walls and in zones of poor mixing in the proximity of the injectors. Hence, we will use Eq. (3) as an estimate the saturation value representative of the mixing conditions.

Figure 2 illustrates the effect of varying the supersaturation ratio in the PSM on the activation of a singly charged ion with a diameter of 2.25 nm ($1/Z=3.70$ V s/cm^2). The curves are the CNC readouts plotted as a function of the inverse of the electrical mobility, determined by the DMA. Note that the fraction of ions that grow into droplets increases as the PSM supersaturation is raised, until a value of S is reached for which the number of counts saturates. We will define the value of S required to activate half of the counts of a given ion as its critical supersaturation $S^*_{50\%}$. An estimate of the resolution with which we measure this critical supersaturation can be obtained from the factor $(1/2)\Delta S/S^*_{50\%}$, where ΔS is the difference between the supersaturation required to detect 80% and 20% of the total particle count of a given ionic peak. This specific deviation-like parameter is very approximately 10% for all the studied embryos, small enough to make our definition of $S^*_{50\%}$

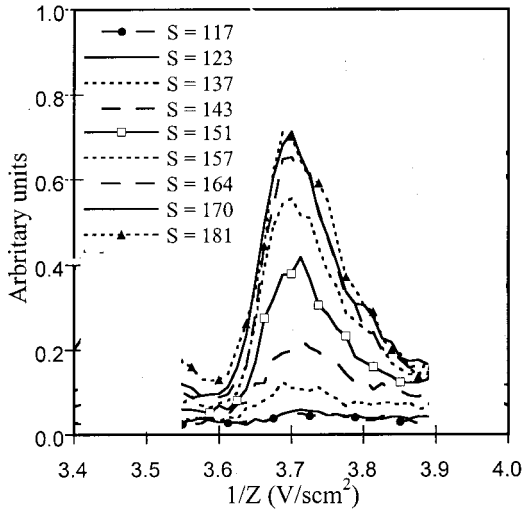

FIG. 2. Activation of an ion as a function of the supersaturation used in the PSM.

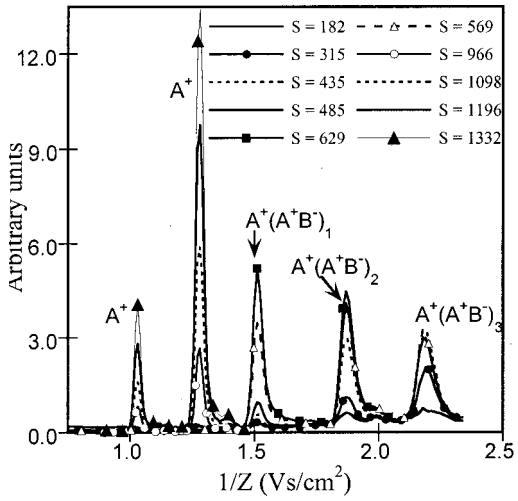

FIG. 3. Supersaturation levels required to activate $A^+(A^+B^-)_n$ ion clusters of different diameters.

meaningful.[13] This small spread in critical supersaturations might be due to a combination of both the energy-activated nature of the ion induced nucleation phenomena, and to small variations of the supersaturation along the mixing channel.

The generation of nanoparticles with different sizes and charge states is a key prerequisite for this nucleation study. Since the pioneering work of Fenn and colleagues, electrospray ionization has proved to be an excellent source of nanoparticles.[22] We have used this technique to generate two different types of nucleation embryos: singly and doubly charged clusters of tetra-alkyl ammonium salts and multiply charged proteins. We have measured the critical supersaturations of seventeen singly charged clusters of tetraheptyl ammonium bromide ($Heptyl_4N^+Br^-$, or A^+B^- hereafter), $A^+(A^+B^-)_n$, with diameters between 0.944 nm and 2.89 nm, as well as the values associated with six doubly charged clusters, $(A^+)_2(A^+B^-)_n$, with diameters between 2.08 nm and 2.54 nm.[23,24] We have also analyzed electrosprays of tetramethyl ammonium hexafluorophosphate, which has a lighter cation, to extend the lower end of the size range of this study. We have not analyzed in detail the sprays of this salt, and cannot establish the exact nature of its ionic peaks. Hence, they will be denoted simply by M_j^+, where j stands for the order of appearance in the mobility spectra. Note that the exact nature of the particle is of little relevance to this study, provided that its charge state and diameter are known, but this point is assured in the case of M_j^+ particles, since the electrosprayed solution contains only monovalent species. In addition, we have electrosprayed two solutions 0.1 mol of ammonium acetate in water, with 100 ppm of the proteins lysolzyme and myoglobine, respectively. The electrospraying of these solutions produces nanoparticles made of 1, 2,..., n individual protein molecules and several unit charges z, Ly_n^{+z}, My_n^{+z}.[13] These particles are ideal to investigate the effect of electric charge on heterogeneous nucleation, since their charge state is easily varied upon partial neutralization, while keeping a constant or almost unaffected diameter.

III. RESULTS AND DISCUSSION

Figures 3 and 4 show the supersaturation values required to activate different nanoparticles. The five most mobile singly charged $Heptyl_4N^+$ clusters are illustrated in Fig. 3. As expected, the values of $S^*_{50\%}$ increase as the embryos' sizes diminish. This rule apparently does not work for the two ionic peaks of larger mobility, which have similar critical supersaturations $S^*_{50\%} \approx 1100$. Recently, de la Mora and Thomson have studied the same spray with a DMA and a mass spectrometer, and determined the mobility and composition of all these charged clusters.[25] They found that the singly charged nanoparticles with mobilities 1.04 and 1.28 V s/cm^2 are indeed the same ion, $Heptyl_4N^+$. Although the large differences in mobility could be due to different geometrical arrangements of the $Heptyl_4$ chains, this explanation seems improvable. Instead, we think that the peak at 1.28 V s/cm^2 is a $Heptyl_4N^+$ ion that has been evaporated between the exit of the DMA and the input of the PSM from a

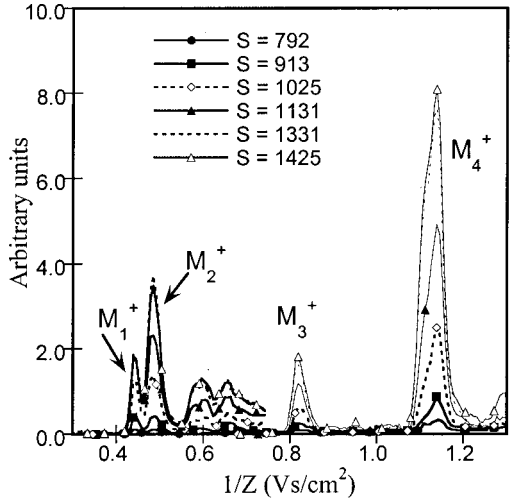

FIG. 4. The critical supersaturation of very small $Methyl_4N^+$ ions does not depend on their diameters.

doubly charged residue having a mobility of 1.28 V s/cm^2. The evaporation of ions from dry residues is similar to the more studied emission from a liquid nanodroplet, with two different ''solvation'' energies controlling each process.[24] Thus, we will consider the two different mobilities of A^+ as an artifact of the experimental technique and assign single values of $1/Z$, mobility diameter, and $S^*_{50\%}$ (1.04 V s/cm^2, 0.94 nm, and approximately 1100) to both A^+ peaks. This finding reduces in one the aggregation degree assigned to the clusters $(A^+)_z(A^+B^-)_n$ reported previously,[17,24] and the correct denomination is used in this work.

Figure 4 shows the saturation spectra of the most mobile nanoparticles produced with the $Methyl_4N^+$-formamide electrospray. Four well resolved ions are observed at 0.44, 0.48, 0.82, and 1.13 V s/cm^2, along with two additional nanoparticle peaks with broader distributions around 0.65 V s/cm^2. The purpose behind this experiment is to determine the critical supersaturation of singly charged ions smaller than A^+. Although we do not know the mass of these ions and, therefore, we cannot establish their composition, the diameters of the most mobile peaks are smaller than that of A^+. In fact, the smallest particle M_1^+ has a mobility diameter of 0.43 nm. Despite this, note that the PSM is able to activate these ions, and it does so at approximately the same critical supersaturation associated with A^+.

All the nucleation data are compiled in Table II. We list the electrical mobility, mobility diameter, charge state, critical supersaturation $S^*_{50\%}$, the temperatures at the mixing channel and the DBP saturator, and the flow rate of nitrogen associated with every nucleation embryo. α and x are rescaled expressions for the critical supersaturation and nanoparticle diameter, which are defined in following paragraphs by Eqs. (9) and (10). The compositions of every singly charged $Heptyl_4N^+$ ion cluster up to $A^+(AB)_5$ and of the doubly charged clusters $(A^+)_2(A^+B^-)_n$ have been determined unambiguously via mass spectrometry.[25] The composition of the remaining $Heptyl_4N^+$ clusters is highly probable. The critical supersaturations of several $A^+(AB)_n$ clusters were measured at two different saturator temperatures, and both results are tabulated. The compositions of the $Methyl_4N^+$ clusters are unknown, although this does not prevent from computing their diameters and charge states. Finally, the structures of the protein aggregates were verified via mobility analysis.[13] Note the wide range of diameter and charge states covered by the data in Table II.

The dependence between critical supersaturation, charge, and diameter of an embryo can be understood with the help of a simple model for the nucleation site and basic results from classical thermodynamics. First, we will assume that the embryo is a spherical particle with its charge located at the center, and that the vapor molecules condense uniformly on its surface forming a sphere of radius R. Second, we will assume that the vapor pressure p of the liquid in this nucleation site is given by the familiar expression for a liquid droplet of radius R (Ref. 26):

$$N_A k_B T \ln\frac{p}{P_\infty} = \left[\frac{\partial W_0}{\partial n}\right]_{T,P}, \tag{4}$$

where P_∞ is the equilibrium vapor pressure for the drop of infinite radius. W_0 stands for the reversible work the system droplet-surrounding vapor is capable of performing, and its partial derivative with respect the molar number of liquid molecules must be done at constant temperature T and pressure P of the vapor phase. Implicit in Eq. (4) is the assumption that the droplet-surrounding vapor is a closed system in equilibrium. Within our approximation, W_0 has two components, surface and electric work, which are given by

$$W_S = 4\pi\gamma R^2, \tag{5}$$

$$W_E = \frac{\epsilon_0}{2}\int\int\int_V \epsilon(\mathbf{x})\mathbf{E}^2 d^3x = \frac{q^2}{8\pi\epsilon_0 R} + \frac{q^2}{8\pi\epsilon_L\epsilon_0}\left(\frac{1}{R_I} - \frac{1}{R}\right), \tag{6}$$

where γ and ϵ_L are the surface tension and dielectric constant of the liquid, and q and R_I the charge and radius of the original embryo. Using these expressions for W_0 and assuming that the surface tension does not depend on the curvature of the drop, Eq. (4) is written as

$$\frac{k_B T}{v_0}\ln\frac{p}{P_\infty} = \frac{2\gamma}{R} - \frac{(1-1/\epsilon_L)q^2}{32\pi^2\epsilon_0 R^4}, \tag{4'}$$

where v_0 is the molecular volume of the liquid. This result was obtained originally by Thomson.[4] The surface tension contributes to augment the equilibrium vapor pressure of any drop of finite size (Kelvin effect), while the presence of electric charge decreases p drastically for large values of the drop's curvature. Finally, we use the Rayleigh radius R_R, the Kelvin radius R_K, and a rescaled supersaturation α,

$$R_R = \left(\frac{(1-1/\epsilon_L)q^2}{64\pi^2\epsilon_0\gamma}\right)^{1/3}, \tag{7}$$

$$R_K = \frac{2\gamma v_0}{k_B T \ln S}, \tag{8}$$

$$\alpha = \frac{R_R}{R_K}, \tag{9}$$

to simplify Eq. (4'),[12]

$$\alpha = \frac{1}{x} - \frac{1}{x^4}, \tag{4''}$$

$$x = \frac{R}{R_R}. \tag{10}$$

Figure 5 contains the nucleation data of Table II in the form of α-x points, along with the traces of Eq. (4'') and Kelvin's radius ($\alpha = 1/x$). Before we analyze the experimental data, let us describe once more the significance of Thomson's equation. Equation (4'') is the locus of equilibrium of the charged drop-surrounding vapor system in the plane x-α. α has a maximum at $x_{\max} = 4^{1/3} \sim 1.587$, $\alpha_{\max} = 3/4^{4/3} \sim 0.472$, which separates two intervals with different equilibrium behaviors. The equilibrium for the branch $x > x_{\max}$ is unstable (Kelvin's effect): if we increase the supersaturation (i.e., α is augmented) in a droplet-vapor system with x-α coordinates on this side of the curve, more vapor will condense and the

TABLE II. Characteristics of the nucleation embryos. We list the inverse of the electrical mobility ($1/Z$), diameter (D), charge state (z), critical supersaturation ($S^*_{50\%}$), rescaled supersaturation (α) and diameter (x), the temperatures of the nucleation chamber (T^*) and saturator (T_S), and the flow rate of nitrogen (Q_N) fed to the PSM. The total flow rate entering the CNC is $Q_O = 2.36\times10^{-5}$ m^3 s^{-1}.

Particle	$1/Z$ (V s/cm^2)	D (nm)	z	$S^*_{50\%}$	α	x	T^* (°C)	T_S (°C)	Q_N ($\times10^6$ m^3 s^{-1})
A^+	1.04	0.944	1	1120, 941	0.468, 0.458	1.02	20.7, 21.2	104.3, 105.7	4.74, 3.87
A^+	1.04 (1.28)	0.944	1	1120, 927	0.468, 0.456	1.02	20.7, 21.2	104.3, 105.7	4.76, 3.74
$(A^+)_1\,(A^+B^-)_1$	1.51	1.25	1	648, 613	0.430, 0.425	1.28	20.0, 19.7	104.3, 105.7	2.46, 2.01
$(A^+)_1\,(A^+B^-)_2$	1.88	1.45	1	359	0.392	1.49	20.5	105.7	1.32
$(A^+)_1\,(A^+B^-)_3$	2.19	1.61	1	266, 365	0.372, 0.391	1.65	20.5, 19.8	105.7, 96.1	0.98, 2.45
$(A^+)_1\,(A^+B^-)_4$	2.46	1.74	1	285	0.375	1.79	19.8	96.1	1.91
$(A^+)_1\,(A^+B^-)_5$	2.83	1.90	1	235	0.362	1.95	19.8	96.1	1.58
$(A^+)_1\,(A^+B^-)_6$	3.14	2.03	1	181	0.344	2.09	19.8	96.1	1.21
$(A^+)_1\,(A^+B^-)_7$	3.43	2.15	1	143, 180	0.329, 0.344	2.21	19.8, 19.6	96.1, 87.4	0.96, 2.32
$(A^+)_1\,(A^+B^-)_8$	3.70	2.25	1	130, 151	0.323, 0.332	2.31	19.8, 19.6	96.1, 87.4	0.87, 1.94
$(A^+)_1\,(A^+B^-)_9$	3.98	2.35	1	115, 133	0.314, 0.323	2.41	19.8, 19.6	96.1, 87.4	0.77, 1.70
$(A^+)_1\,(A^+B^-)_{10}$	4.24	2.45	1	103, 119	0.307, 0.316	2.52	19.8, 19.6	96.1, 87.4	0.69, 1.53
$(A^+)_1\,(A^+B^-)_{11}$	4.50	2.54	1	96, 111	0.303, 0.311	2.61	19.8, 19.6	96.1, 87.4	0.64, 1.42
$(A^+)_1\,(A^+B^-)_{12}$	4.74	2.62	1	102	0.306	2.69	19.6	87.4	1.31
$(A^+)_1\,(A^+B^-)_{13}$	4.99	2.70	1	94.7	0.301	2.77	19.6	87.4	1.22
$(A^+)_1\,(A^+B^-)_{14}$	5.21	2.77	1	89.3	0.297	2.85	19.6	87.4	1.15
$(A^+)_1\,(A^+B^-)_{15}$	5.41	2.83	1	87.3	0.296	2.91	19.6	87.4	1.12
$(A^+)_1\,(A^+B^-)_{16}$	5.59	2.89	1	84.2	0.293	2.97	19.6	87.4	1.08
$(A^+)_2\,(A^+B^-)_5$	1.64	2.08	2	137	0.517	1.35	19.6	87.4	1.76
$(A^+)_2\,(A^+B^-)_6$	1.80	2.21	2	118	0.501	1.43	19.6	87.4	1.52
$(A^+)_2\,(A^+B^-)_7$	1.87	2.26	2	101	0.485	1.46	19.6	87.4	1.30
$(A^+)_2\,(A^+B^-)_8$	2.01	2.36	2	86.6	0.469	1.53	19.6	87.4	1.11
$(A^+)_2\,(A^+B^-)_9$	2.13	2.45	2	83.3	0.465	1.59	19.6	87.4	1.07
$(A^+)_2\,(A^+B^-)_{10}$	2.26	2.54	2	80.7	0.461	1.64	19.6	87.4	1.04
M_1^+	0.443	0.435	1	1020	0.462	0.45	20.5	104.3	4.22
M_2^+	0.484	0.477	1	1080	0.465	0.49	20.5	104.3	4.44
M_3^+	0.819	0.782	1	1090	0.465	0.80	20.5	104.3	4.47
M_4^+	1.13	1.01	1	1060	0.464	1.04	20.5	104.3	4.38
Ly_1^{+1}	9.05	3.75	1	33.1	0.238	3.84	23.9	69.9	2.74
Ly_1^{+2}	4.80	3.88	2	32.4	0.373	2.50	23.1	69.9	2.40
Ly_2^{+1}	13.9	4.77	1	21.2	0.206	4.89	22.6	69.9	1.46
Ly_2^{+2}	7.15	4.85	2	19.2	0.317	3.13	22.6	69.9	1.32
Ly_3^{+1}	17.8	5.47	1	13.3	0.174	5.61	22.6	69.9	0.91
Ly_3^{+2}	9.10	5.54	2	13.1	0.275	3.58	22.6	69.9	0.90
Ly_4^{+1}	21.3	6.03	1	10.1	0.156	6.18	22.6	69.9	0.70
Ly_4^{+2}	10.9	6.10	2	9.3	0.239	3.94	22.6	69.9	0.64
Ly_5^{+1}	24.5	6.51	1	8.0	0.140	6.67	22.6	69.9	0.55
My_1^{+1}	9.72	3.90	1	36.3	0.243	4.00	23.0	73.8	1.83
My_1^{+2}	5.09	4.01	2	31.7	0.371	2.59	23.0	73.8	1.60
My_1^{+3}	3.4	4.01	3	26.6	0.461	1.98	23.0	73.1	1.43
My_1^{+4}	2.7	4.14	4	21.2	0.520	1.69	23.0	73.1	1.15
My_1^{+5}	2.20	4.19	5	18.6	0.578	1.47	23.0	73.1	1.00
My_2^{+2}	7.54	4.99	2	16.7	0.302	3.22	23.0	73.85	0.84

droplet size will augment indefinitely as long as vapor is available. On the other hand, the equilibrium of branch $x < x_{\max}$ is stable: if the supersaturation of a system located on this side of the curve is increased, the radius of the embryo-condensed vapor droplet will grow to a stable x value given by Eq. (4″) and the new α. If the supersaturation is increased beyond $\alpha_{\max}$, the nucleation site becomes unstable and grows indefinitely.

From the reading of the original work, it appears that Thomson was only concerned with applying Eq. (4*rr*) to the nucleation of ions smaller than $x_{\max}$, and did not use his equation to deal with the general case including larger embryos. The branch of Thomson's equation associated with stable equilibrium, $x < x_{\max}$, has been employed to estimate the diameter of prenucleation clusters or stable particles formed by an embryo and a few condensed vapor molecules.[11,27] Nevertheless, Thomson's assumptions should fail for many clusters with diameters much smaller than $x_{\max}$: as indicated by Eq. (4), the equilibrium vapor pressure of the cluster is determined by the derivative of its Gibbs free energy with respect to the number of condensing vapor molecules. In the case of a nucleation cluster with a ''thick'' layer of condensed vapors, the characteristics of the embryo, other than its charge, have little influence in the change of

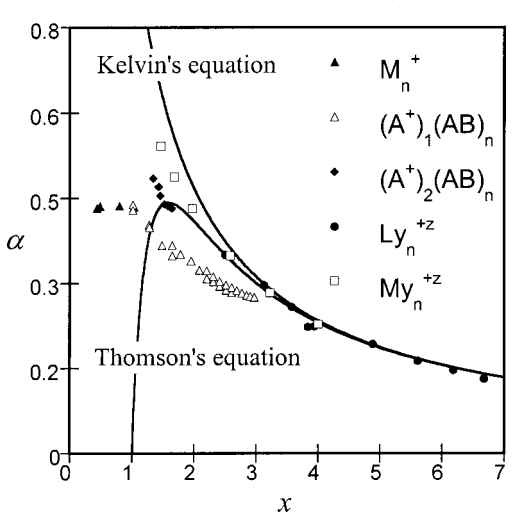

FIG. 5. Critical supersaturation values associated with the embryos in α-x space. Thomson's and Kelvin's criteria are also plotted.

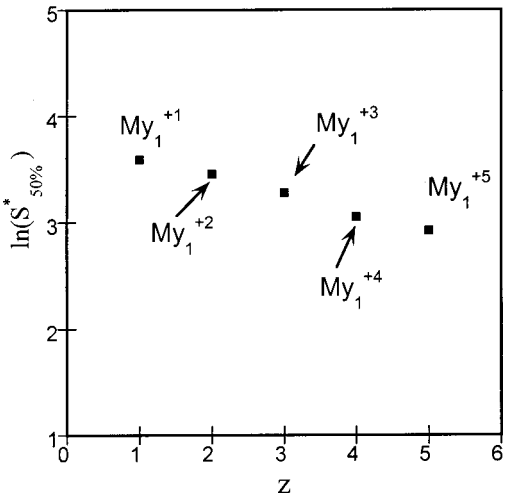

FIG. 6. Plot of $\ln(S^*_{50\%})$ versus charge state of myoglobine monomers. Their dependence appears lineal rather than quadratic.

the Gibbs free energy induced by the arrival of one additional vapor molecule (the ''thick'' layer shields the particularities of the embryo), and the use of Eqs. (5) and (6) to calculate the Gibbs free energy of the cluster is justified. However, these formulas are inaccurate for smaller prenucleation clusters.

Despite the simplicity of Thomson's model, it is observed that a significant fraction of the experimental data in Fig. 5 agrees fairly well with this theory. The most striking coincidence is that the supersaturations required to activate the five smallest singly charged ions are practically identical ($\alpha \sim 0.463$) and very similar to $\alpha_{\max}$. As mentioned above, the nucleation on these small ions is the case that resembles better Thomson's simple model: because of the small size of the original embryo, a layer of liquid of considerable thickness must be formed before the nucleation site becomes unstable and grows indefinitely. This layer shields the particularities of the ionic core (e.g., actual location of the ionic charge and embryo-vapor interacting potentials other than Coulombic), and the incoming vapor molecules condense on the nucleation site very much like if it were a liquid droplet with a central electric charge equal to that of the embryo. Another significant agreement is observed with the largest particles holding one unit charge, which fall on top of Thomson's curve. The effect of one elementary charge on the activation of these proteins is small, and the most reliable and confirmed Kelvin's criterion is expected to hold accurately in this diameter range. Incidentally, the match between theory and empirical data for these relatively large particles confirms the validity of the supersaturation values measured in the PSM.

Figure 5 also shows that the activation of many embryos does not follow Thomson's model exactly. The most obvious cases are the multiply charged nanoparticles, which require much higher supersaturation values than predicted by Eq. (4″). In fact, the proteins with highest charge states fall closer to the curve associated with the Kelvin's radius. The disagreement is most noticeable for $(A^+)_2(A^+B^-)_5$, $(A^+)_2(A^+B^-)_6$, My_1^{+5}, and My_1^{+4}, which are activated at α values well above $\alpha_{\max}$. The cause for this discrepancy seems to be the effect of the electric charge held by these larger nanoparticles on the nucleation, which is not well described by the simple geometrical model of Thomson. To show this we have plotted in Fig. 6 the values of $\ln(S^*_{50\%})$ versus the charge number for the myoglobine clusters containing a single protein molecule. Because these embryos have the same diameter, the points in Fig. 6 should follow a parabola according to Eq. (4′). However, the experimental trend is quite linear. We believe that this paradox is due to the actual geometry of the multiply charged embryos, which is determined by the process of formation of the nanoparticles: any of these clusters is the result of a liquid droplet with a neutral residue core (the matter of the future embryo) and a few individual surface charges. The liquid evaporates eventually, living behind the dry residue with electric charges on its surface at equidistant locations. When the molecules of the supersaturated vapor condense on the surface of one of these multiply charged nanoparticles, it seems reasonable to assume that they will distribute preferentially around the electric charges favored by ion-dipole interactions. It is also probable that the ''large'' nucleation site will reach the state of unsteady equilibrium before a homogeneous layer of condensed vapor shields the asymmetries of the embryo. In this case, Thomson's model would fail to describe the activation of these particles (there is not a central electric field), and the dependence of $\ln(S^*_{50\%})$ on the embryo's charge state would be linear rather than quadratic.

Note also that the singly charged $\text{Heptyl}_4\text{N}^+$ clusters larger than A^+ are activated at values of $S^*_{50\%}$ slightly lower than predicted by Eq. (4″). This small discrepancy might also be due to asymmetries of the nucleation site: the location of the charge on the particle's surface and a likely partial or thin condensation layer previous to the embryo's activation preclude the formation of a central electric field. A second factor causing the disagreement could be embryo-vapor interaction potentials other than Coulombic, which could be important in the case of a thin condensed layer, and which are not considered in Thomson's model.

Before this section ends, it is necessary to comment on how our results compare to previous cloud chamber data. Unfortunately, such a comparison is difficult because the definitions of the critical supersaturation used in the present work and that adopted in cloud chamber experiments are different. Here, the critical supersaturation associated with a given embryo is defined as the supersaturation required to activate one-half of the total number of embryos, $S^*_{50\%}$; such a definition is useful because it makes possible a comparison with Thomson's theory. The nucleation of embryos is a kinetic process: typically, a supersaturation value S_0 defines an equilibrium distribution of solvated ions (prenucleation embryos) and grown droplets (the latter are the ''activated ions'' or ions that have grown by condensation beyond a critical size). The concentration of activated ions is proportional to $\exp(-\Delta G/k_BT)$, where the energetic barrier ΔG is the difference in free energies between the ion of critical size and the most abundant solvated ion associated with the supersaturation S_0. Thomson's equation can be used to compute the free energy of solvated ions, especially for the larger ones, including that of critical size.[6] When the critical supersaturation for the activation of a population of ions is defined as that value required to activate most ions of the population (this is the definition used in the present work, as well as the definition implicit in Thomson's theory), this critical supersaturation condition implies that ΔG must be small or, in other words, the critical supersaturation $S^*_{50\%}$ must be close to the supersaturation associated with the ion of critical size (a value given by Thomson's theory). On the other hand, the critical supersaturation of cloud chamber experiments, S_{CC}, is customary defined as the value of the maximum saturation within the chamber for which the rate of generation of detectable droplets is 1 $\mathrm{cm}^{-3}\,\mathrm{s}^{-1}$.[8–10] Depending on the experimental conditions, S_{CC} may be much smaller than the supersaturation associated with the critical embryo: if the rate of generation of ions in the cloud chamber is very high (much larger than 1 $\mathrm{cm}^{-3}\,\mathrm{s}^{-1}$), low values of the supersaturation may induce a rate of nucleation of the order of 1 droplet $\mathrm{cm}^{-3}\,\mathrm{s}^{-1}$. This reasoning indicates that published values of S_{CC} might be significantly smaller than our measurements of $S^*_{50\%}$. A second feature of cloud chambers experiments that handicap the comparison with our data is the lack of characterization of the embryos. This is true for every cloud chamber study with the exception of the work of Kane and colleagues, which uses resonant enhanced multiphoton ionization to seed a cloud chamber with ions of well-known composition.[10,11,28] Even for the latter case, it is apparent that previous cloud chamber results were limited to the study of the nucleation of small ions ($x<1.587$), which represents only a fraction of the size range studied in the present work.

IV. CONCLUSION

The combination of electrospray ionization, a high-resolution differential mobility analyzer, and a turbulent-mixing condensation chamber of variable supersaturation makes it possible to study accurately the critical supersaturation required to activate electrified nanoparticles of varying size a charge state. We have undertaken this investigation using a variety of nanoparticles with diameters ranging from 0.43 nm to 6.51 nm, and having up to +5 unit charges. We have found that the smallest ions characterized in this paper, $0.43\ \mathrm{nm}<D<1.01\ \mathrm{nm}$, are activated with DBP vapors at approximately the same supersaturation regardless of their size (at constant nucleation temperature). From the point of view of analytical applications, this result is important because it confirms that charged nanoparticles of arbitrary small sizes can be optically counted and provides for a method to do so.[13] Furthermore, the critical supersaturation associated with these small ions coincides with the classical result derived by Thomson.[4] This theory is also a good guidance to estimate the critical supersaturation of larger singly charged embryos, although it fails to predict the activation of multiply charged nanoparticles. The discrepancy is significant for the larger protein clusters: although their charge states, according to Thomson's equation, are high enough to induce a noticeable effect in the nucleation, their critical supersaturations are better predicted by Kelvin's criterion, in which the electrification of the embryo plays no role. We believe that this disagreement is due to the geometry of our multiply charged embryos, with charge sites spread on their surface. This configuration probably promotes localized condensation around the individual charges and prevents a central distribution of the electric field on the surface of the nucleating embryo, which is a main assumption of Thomson's theory.

[1] S. K. Friedlander, *Smoke, Dust, and Haze: Fundamentals of Aerosol Dynamics*, 2nd ed. (Oxford University Press, New York, 2000).
[2] F. Q. Yu and R. P. Turco, J. Geophys. Res., [Atmos.] **106**, 4797 (2001).
[3] P. H. McMurry, Aerosol. Sci. Technol. **33**, 297 (2000).
[4] J. J. Thomson, *Conduction of Electricity through Gases* (Dover, New York, 1969).
[5] I. Kusaka, Z. G. Wang, and J. H. Seinfeld, J. Chem. Phys. **103**, 8993 (1995).
[6] A. W. Castleman and I. N. Tang, J. Chem. Phys. **57**, 3629 (1972).
[7] A. W. Castleman, P. M. Holland, and R. G. Keesee, J. Chem. Phys. **68**, 1760 (1978).
[8] H. Rabeony and P. Mirabel, J. Phys. Chem. **91**, 1815 (1987).
[9] F. He and P. Hopke, J. Chem. Phys. **99**, 9972 (1993).
[10] D. Kane, G. Daly, and M. S. El-Shall, J. Phys. Chem. **99**, 7867 (1995).
[11] D. Kane, M. Rusyniak, S. P. Fisenko, and M. S. El-Shall, J. Phys. Chem. **104**, 4912 (2000).
[12] T. Seto, K. Okuyama, L. de Juan, and J. Fernández de la Mora, J. Chem. Phys. **107**, 1576 (1997).
[13] M. Gamero-Castaño and J. Fernández de la Mora, J. Aerosol Sci. **31**, 757 (2000).
[14] M. Gamero-Castaño and V. Hruby, J. Propul. Power **17**, 977 (2001).
[15] J. Fernández de la Mora and I. G. Loscertales, J. Fluid Mech. **260**, 155 (1994).
[16] M. Cloupeau and B. Prunet-Foch, J. Electrost. **22**, 135 (1989).
[17] M. Gamero-Castaño and J. Fernández de la Mora, Anal. Chim. Acta **406**, 76 (2000).
[18] T. Eichler, Senior Graduation thesis, Fachhochscule Offenburg, Germany, 1997.
[19] H. Tammet, J. Aerosol Sci. **26**, 459 (1995).
[20] J. Fernández de la Mora, L. de Juan, T. Eichler, and J. Rosell, Trends Anal. Chem. **17**, 328 (1998).
[21] K. Okuyama, Y. Kousaka, and T. Motouchi, Aerosol. Sci. Technol. **3**, 353 (1984).
[22] J. B. Fenn, M. Mann, C. K. Meng, S. K. Wong, and C. Whitehouse, Science **246**, 64 (1989).
[23] M. Gamero-Castaño and J. Fernández de la Mora, Anal. Chem. **72**, 1426 (2000).

[24] M. Gamero-Castaño and J. Fernández de la Mora, J. Mass Spectrom. **35**, 790 (2000).
[25] J. Fernández de la Mora and B. Thomson (unpublished).
[26] H. Reiss, *Methods of Thermodynamics* (Blaisdell, New York, 1965).
[27] J. M. Makela, M. Riihela, A. Ukkonen, V. Jokinen, and J. Keskinen, J. Chem. Phys. **105**, 1562 (1996).
[28] D. Kane, S. P. Fisenko, and M. S. El-Shall, Chem. Phys. Lett. **277**, 13 (1997).